Accepted Manuscript

Atomic layer deposition of Pt@CsH_2PO_4 for the cathodes of solid acid fuel cells

Dae-Kwang Lim, Jian Liu, Shobhit A. Pandey, Haemin Paik, Calum R.I. Chisholm, Joseph T. Hupp, Sossina M. Haile

PII: S0013-4686(18)31577-9

DOI: 10.1016/j.electacta.2018.07.076

Reference: EA 32273

To appear in: *Electrochimica Acta*

Received Date: 3 December 2017

Revised Date: 10 July 2018

Accepted Date: 13 July 2018

Please cite this article as: D.-K. Lim, J. Liu, S.A. Pandey, H. Paik, C.R.I. Chisholm, J.T. Hupp, S.M. Haile, Atomic layer deposition of Pt@CsH_2PO_4 for the cathodes of solid acid fuel cells, *Electrochimica Acta* (2018), doi: 10.1016/j.electacta.2018.07.076.

Atomic Layer Deposition of Pt@CsH_2PO_4 for the Cathodes of Solid Acid Fuel Cells

Dae-Kwang Lim,[a] Jian Liu,[b] Shobhit A. Pandey,[a] Haemin Paik,[a,c] Calum R.I. Chisholm,[d] Joseph T. Hupp,[b] Sossina M. Haile,[*,a]

[a] Department of Materials Science and Engineering, Northwestern University, 2220 Campus Drive, Evanston, IL 60208, USA

[b] Department of Chemistry, Northwestern University, 2220 Campus Drive, Evanston, IL 60208, USA

[c] Materials Science, California Institute of Technology, 1200 California Blvd., Pasadena, CA 91125, USA

[d] SAFCell Inc., 36 S. Chester Ave., Pasadena, CA 91106, USA

*corresponding author: sossina.haile@northwestern.edu

Graphical abstract

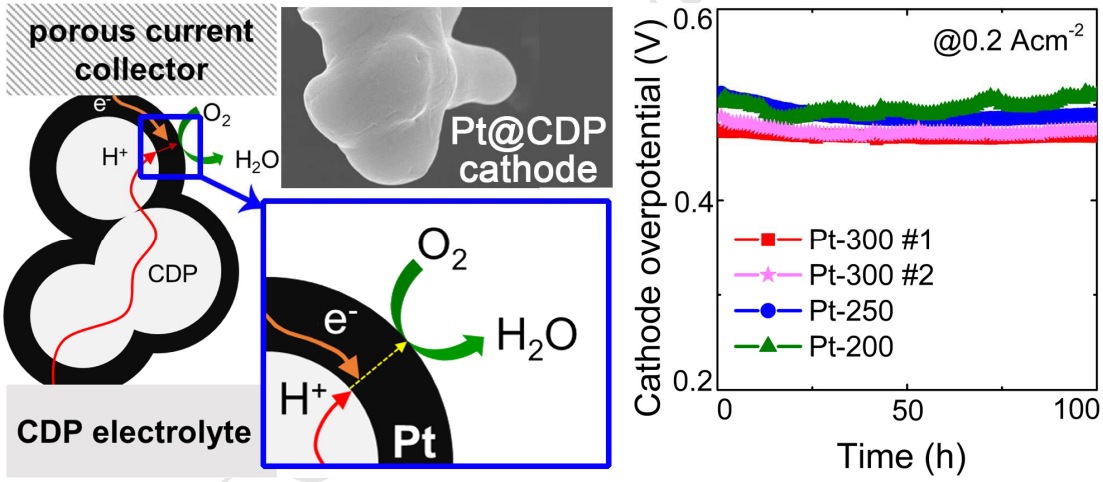

Abstract

Atomic layer deposition (ALD) has been used to apply continuous Pt films on powders of the solid acid CsH_2PO_4 (CDP), in turn, used in the preparation of cathodes in solid acid fuel cells (SAFCs). The film deposition was carried out at 150 °C using trimethyl(methylcyclopentadienyl)platinum ($MeCpPtMe_3$) as the Pt source and ozone as the reactant for ligand removal. Chemical analysis showed a Pt growth rate of 0.09 ± 0.01 wt%/cycle subsequent to an initial nucleation delay of 84 ± 20 cycles. Electron microscopy revealed the contiguous nature of the films prepared using 200 or more cycles. The cathode overpotential (0.48 ± 0.02 V at a current density of 200 mA/cm^2) was independent of Pt deposition amount beyond the minimum required to achieve these continuous films. The cell electrochemical characteristics were moreover extremely stable with time, with the cathode overpotentials increasing by no more than 10 mV over a 100 h period of measurement. Thus, ALD holds promise as an effective tool in the preparation of SAFC cathodes with high activity and excellent stability.

Keywords: Solid acid fuel cell; Atomic layer deposition; CsH_2PO_4; Platinum film

1. **Introduction**

Solid acid fuel cells (SAFCs) are a relatively new class of fuel cells which employ the proton conductor cesium dihydrogen phosphate (CsH_2PO_4 or CDP) as the electrolyte. This material undergoes a transition to a superprotonic phase at 228 °C, at which the conductivity rises by several orders of magnitude to ~ 10^{-2} S/cm.[1] The behaviour has enabled fuel cell operation at ~ 250 °C.[2] Like other fuel cells, SAFCs offer the benefits of clean, quiet, and

efficient conversion of chemical fuels to electricity. Beyond these typical fuel cell characteristics, SAFCs offer advantages as a consequence of operation at an intermediate temperature. Specifically, at 250 °C electrocatalysis rates are high in comparison to those under ambient conditions, resulting in a high tolerance for typical fuel impurities such as CO and H_2S, while relatively inexpensive materials can be utilized as auxiliary components. Despite these features, widespread adoption of SAFCs remains elusive, largely because of poor performance characteristics of the cathode. Achieving acceptable SAFC power outputs (i.e., peak power densities approaching 200 mW/cm^2)[3] has required high Pt loadings, on the order of 2 mg/cm^2,[4] and cathode microstructural evolution has been implicated in cell degradation.[3, 4] In turn, these factors imply system costs in excess of the $1000/kW target typically quoted for entry into early commercial markets.

The first studies of SAFCs employed mechanical mixtures of ionic (the electrolyte) and electronic (Pt black and Pt on carbon) components.[5, 6] While essential at that time for demonstrating proof-of-concept with an easily fabricated cell, the approach resulted in excessive Pt loadings, ranging from 8 to 18 mg/cm^2 in the cathode alone. A breakthrough in electrode processing was realized by Papandrew and colleagues, who recognized that Pt connectivity and utilization in SAFC cathodes could be dramatically enhanced by application of a thin film of Pt onto fine CDP particles.[4] These coated particles (Pt@CDP) were then lightly pressed to generate a porous structure with an interconnected electronic conduction pathway. The architecture benefitted not only from the reduced Pt loading, but also from the absence of any form of carbon, which can otherwise react with oxygen and result in cell degradation.[7] Application of the Pt coating was pursued by these authors using an atypical MOCVD (metal organic chemical vapor deposition) strategy in which platinum acetylacetonate ($Pt(acac)_2$), the Pt

precursor, was simply milled together with CDP, and the mixture heat-treated at a temperature high enough to induce vaporization of the precursor and its decomposition on the CDP surface. The procedure generated a thin Pt coating onto the CDP particles, the approximate thickness of which was controlled simply by controlling the relative amounts of $Pt(acac)_2$ and CDP. While attractive in terms of low cost and ease of implementation, such an approach does not lend itself to precise control of Pt morphology. In turn, this suggests challenges in tuning the process for optimal Pt utilization and in using such structures for elucidating the critical factors determining the oxygen reduction rate. Furthermore, degradation of the cathode created by this process was noted as a remaining challenge.[4]

Atomic layer deposition (ALD) has emerged as a remarkable process for deposition of conformal films of a wide variety of materials on an equally wide variety substrates.[8] The self-limiting adsorption behaviour of the reactants used in the process affords exquisite control of film thickness. While preparation of metallic films by ALD is less developed than that of oxides, several reports of Pt growth appear in the literature,[9] suggesting its suitability as a method for obtaining Pt coated CDP. These prior studies use as the metal precursor either ($Pt(acac)_2$) or (methylcyclopentadienyl)trimethylplatinum ($MeCpPtMe_3$), and as the oxidant, either O_2, oxygen plasma, or O_3 (ozone).[10, 11] Here we select $MeCpPtMe_3$ and ozone for Pt deposition on CDP because growth temperatures as low as 100 °C with growth rates on the order of 0.45 Å/cycle have been demonstrated for this combination.[11] These conditions are compatible with CDP, which unless held under high steam partial pressures, undergoes a slow and highly detrimental dehydration/decomposition reaction at temperatures above ~150 °C.[12] We examine the impact of varying the number of ALD cycles on both deposition characteristics and fuel cell polarization behaviour.

2. Experimental Procedures

2.1 ALD of Pt on CDP

Powders of CDP with specific surface area of 2.4 m^2/g were prepared in-house by aqueous routes using cesium carbonate (Alfa Aesar, 99.9%) and phosphoric acid (Fisher Scientific, 85%) as the starting materials.[4] ALD preparations were carried out using a pulse type Savannah 100 reactor (Cambridge Nanotech, Inc.) with 80 mg of CDP powders loaded into the reactor for each deposition. Prior to the delivery of reactant gases, the CDP was vacuum heat-treated for 30 min at 150 °C to remove any physisorbed water. The CDP powder was then held at 150 °C for the subsequent deposition. The solid platinum precursor was pulsed at a temperature of 75 °C, using ultra-high purity nitrogen as the carrier, which also served as the purge gas. Each deposition cycle consisted of the following five steps: (1) 1 s pulse of $MeCpPtMe_3$; (2) 220 s hold to provide time for the precursor to diffuse throughout the powder; (3) 220 s N_2 purge; (4) 45 s pulse of O_3; (5) 45 s N_2 purge. This sequence of ALD steps was then repeated, between 100 and 450 times. Sample nomenclature hereafter follows the system Pt-xxx, where xxx is the number of cycles. The Pt-100 and Pt-200 preparations were duplicated to evaluate reproducibility.

2.2 Physical characterization

The quantity of Pt deposited onto the CDP powders was determined using Inductively Coupled Plasma Optical Emission Spectroscopy (ICP-OES, Thermo iCAP 7600) with sub ppm detection levels. Samples of the Pt@CDP material were placed in a 10% vol/vol acid solution with a 1:1 volume ratio of trace metal grade HCl : HNO_3 in Millipore water, with a solids

concentration of 10 mg of solids in a 10 ml solution. Complete digestion, yielding a clear, pale yellow solution, was achieved after sonicating the solution for 15 min at room temperature and then holding it at 60 °C for 48 hours.

The surface morphology of the CDP powders before and after Pt coating was examined by field-emission scanning electron microscopy (FE-SEM; Hitachi SU8030 and Hitachi S-4800). In some cases, for direct visualization of the morphology of the Pt layer, the underlying CDP was dissolved away in water. The residual Pt films so obtained were imaged by FE-SEM (as above) and/or by transmission electron microscopy (TEM; Hitachi HD2300 and Hitachi H8100). The Pt@CDP powders were further characterized by X-ray diffraction (XRD; D/MAX Ultima, Rigaku) using Cu Kα radiation at a scan rate of 5°/min. Diffraction data were collected from both as-prepared powders and powders extracted from fuel cell cathodes after prolonged electrochemical measurements.

2.3 Fuel cell preparation and electrochemical characterization

Anode-supported electrochemical cells, 1.9 cm in diameter, were prepared using the Pt@CDP powders in the cathode following procedures similar to those described elsewhere.[4, 6] In brief, the anode electrocatalyst layer is 25 mg of a mixture of CsH_2PO_4 + Pt on carbon (20 mass% Pt on carbon black, HiSPEC® 3000, Alfa Aesar) in a 6:1 mass ratio. This layer is supported on 75 mg of a mixture of CsH_2PO_4 + carbon black acetylene (Alfa Aesar, 99.9%) + naphthalene (Alfa Aesar, 99.8%) in a 3:1:2 mass ratio, where the naphthalene serves as a fugitive pore former. The anode bilayer, in turn, supports a ~ 50 μm thick dense electrolyte layer. Complete fuel cells were prepared by spreading between 33 and 50 mg of the cathode powder over the entire area of a half-cell, and then applying a top layer of carbon paper (TGP-H-120

Toray paper) to serve as a gas diffusion layer and cathode-side current collector. The entire structure was lightly pressed to adhere the layers to one another without closing the electrode porosity. Pt loadings in the cathode ranged from 0.1 to 4.1 mg/cm^2, as described below.

For electrochemical characterization, cells were sealed into an in-house constructed fuel cell test station.[6] Fuel cell polarization curves and impedance spectra were collected at 250 °C after thermal equilibration. Cathode and anode were respectively supplied with humidified (pH$_2$O = 0.38 atm) high purity hydrogen at a flow rate of 30 sccm and with humidified synthetic air at a flow rate of 75 sccm. Data were recorded using a BioLogic SP-300 potentiostat configured with an integrated frequency response analyser. Impedance spectra were collected over the frequency range 0.1 to 10^6 Hz without and with a bias of 200 mA/cm^2. Without bias, the spectra were recorded using a voltage amplitude of 20 mV; with bias, they were recorded using a current amplitude of 10 mA. Polarization curves were obtained every hour over a period of 100 hours, by scanning the voltage from 1 to 0 V at a rate of 10 mV/s; the open circuit voltage (OCV) was in all cases below 1 V and thus the full range of cell voltages was captured. Between measurements, cells demonstrating high current densities were held at a fixed bias of 200 mA/cm^2, whereas those of low performance were held at OCV. The electrode overpotential was determined from the raw polarization curves by subtraction of the ohmic loss determined from impedance spectroscopy and the measured voltage from the expected Nernst potential of 1.116 V. The latter is computed on the basis of the fuel cell measurement conditions. Impedance measurements of symmetric cells with anode components on both sides and exposed to hydrogen at both electrodes showed negligible electrochemical resistance to the hydrogen electrooxidation reaction (~ 0.05 Ωcm^2), and thus the entirety of the electrode overpotential was assigned to the

cathode (i.e., the anode serves as a pseudo-reference). Further details are provided in the Supplementary Information (Figure S1).

3. Results and Discussion

Deposition of Pt on CDP powders was successfully achieved, with amounts ranging from 0.6 to 30 wt% Pt for the range of cycle numbers utilized (100 – 450), Figure 1. The Pt yield, a comparison of the quantity of Pt supplied to the system to the quantity deposited on the powder, is below 1% (ranging from ~ 0.5% for Pt-100 to ~ 0.8% for Pt-300). The Pt growth was found to occur in a two-stage process as evidenced, not only from the amount of Pt deposited as a function of the number of cycles, but also the SEM imaging, Figures 2 and Supplementary Figure S2, and the diffraction patterns, Figure 3. In the first stage, of about 80 cycles, minimal deposition occurred. Specifically, after 100 ALD cycles an average of only 1.5 wt% Pt was deposited (Figure 1). Moreover, for the Pt-100 materials with 0.56 wt% Pt, the metal was essentially undetectable in the X-ray diffraction pattern (Figure 3), and the SEM image, Figure 2b, reveals the presence of isolated Pt nanoparticle clusters on the surface of the large CDP particles. In the second stage, the deposition amount varied linearly with the number of ALD cycles. The deposition behaviour was found to be reasonably reproducible, as indicated by the low scatter in the data (R^2 = 0.93). Unless stated otherwise, the samples with lesser Pt amounts from the two duplicated depositions, Pt-100 and Pt-200, were used for subsequent studies, including the SEM imaging and diffraction analysis (Figures 2 and 3).

We attribute the two-stage deposition behaviour of Pt on CDP to a nucleation delay prior to the onset of layer-by-layer growth. An incubation period for ALD growth of metals onto

oxides has been observed in many systems, and is not surprising here.[13-16] During the incubation period, rather than the deposition of uniform, monoatomic layers of the metal, isolated nanoparticles, as exemplified in Figure 2b, are formed as a result of the high surface energy between substrate and deposit. These nuclei undergo very slow lateral growth (or additional nuclei are formed at a slow rate), until a continuous film is eventually attained. Linear growth occurs in the second stage, consistent with the self-limiting nature of the ALD process. The growth rate of Pt on CDP in this latter regime is found to be 0.09 ± 0.01 wt% cycle, which corresponds to ~ 0.02 nm/cycle, as estimated on the basis of the CDP specific surface area of 2.4 m^2/g. The zero growth intercept is 84 ± 20 cycles. The transition between films with discontinuous and continuous morphology as a function of number of ALD cycles is not sharp. Specifically, the SEM image of the Pt-150 material, with a Pt content of 3.2 wt%, reveals a Pt film that is generally interconnected, though clearly not yet continuous (Figure 2c, e). After 200 cycles, the resulting film is entirely continuous (Figure 2d); a large defect in the free-standing Pt-200 film (Figure 2f) is a result of the handling involved in removal by dissolution of the underlying CDP. As a consequence of the limited thickness of the films (Figure 2f), the micron scale surface morphology of the Pt@CDP is largely unchanged from that of the neat CDP material.

The slight variation in the deposition efficiency observed in the Pt-100 and Pt-200 experiments is attributed to variations in the nature of the CDP surface, which would likely impact the nucleation characteristics. In addition, variation in the precursor vapor pressure, as a consequence of depletion of the source tank, may have played a role. This result indicates that in order to capitalize on the precise control of film thickness otherwise offered by ALD, enhanced control of the Pt nucleation behaviour and process parameters may be desirable.

X-ray diffraction analysis of the Pt@CDP materials, Figure 3, revealed that no phase other than Pt or CDP emerged from the processing. Beyond confirming the successful deposition of Pt, the results imply that CDP is robust against exposure to ozone at 150 °C. Furthermore, the diffraction peaks due to Pt are broad, indicating a small crystallite size. On the basis of the Scherrer equation,[17] the average Pt crystallite sizes in the Pt-200, Pt-250 and Pt-300 powders are estimated to be 8, 10, and 12 nm, respectively, surprisingly larger than the estimated film thicknesses. Transmission electron microscopy images of the Pt-200 free-standing film, Figure 4, corroborate both the SEM observation of a highly continuous film after 200 cycles of deposition and the XRD peak breadth analysis of the crystallite size, found by TEM to be also approximately 8 nm. The selected area diffraction pattern confirms that the film is crystalline Pt, but it was not possible to independently estimate the film thickness from these microscopy studies. How a crystallite size of 8 nm is achieved in a film with an estimated thickness of 1.8 nm is not immediately evident. The result may reflect a highly corrugated Pt film, morphologically highly anisotropic Pt grains, or a loss of CDP surface area during ALD processing.

Fuel cell cathodes were prepared from five of the ALD synthesis batches with deposition cycles between 100 and 300, with two cells prepared from the Pt-300 batch. As noted above, for the Pt-100 and Pt-200 depositions, the powder batches that resulted in lower Pt depositions were utilized for fuel cell studies. The relevant characteristics of the Pt@CDP powders utilized in the present fuel cell studies are summarized in Table 1. Papandrew *et al.* [4] have suggested that Pt film thickness is an important parameter in defining the polarization behaviour of SAFC cathodes prepared using Pt@CDP powders. For a specific surface area of CDP of ~ 2.4 m^2/g, the average Pt thickness implied by the Pt deposition amounts are between 0.1 and 5.9 nm, and the

value for each of the cathode catalyst powders is also included in the table. Raw polarization curves and impedance spectra are reported in Supplementary Figure S3.

The cathode overpotentials, as recorded after 100 h of operation, Figure 5, were found to be remarkably similar for the cells incorporating Pt-200, Pt-250, and Pt-300 powders in the cathode. The overall area-normalized cell resistance values under 200 mA/cm^2 bias range between 0.8 and 1.1 Ωcm^2, of which about 0.5 Ωcm^2 is readily assigned to the electrodes, Figure S3. The latter greatly exceeds the 0.05 Ωcm^2 attributed to the anode, justifying the identification of the anode as a pseudoreference. Returning to the specifics of the cathode characteristics, even a substantial variation in cathode mass was found to have no significant impact on cathode overpotential, as evidenced by the similarity of the results of the two Pt-300 based cells, one prepared using 37 mg and the other using 50 mg of Pt@CDP. This suggests that the active region lies well within 80 μm of the electrolyte-cathode interface (where 80 μm is the thickness of the 37 mg cathode). It is further noteworthy that the overpotential is insensitive to the Pt crystallite size, which spans from 8 nm in Pt-200 to 12 nm in Pt-300.

In contrast to cells prepared from Pt@CDP powders of 200 or more ALD cycles, those prepared from Pt-100 and Pt-150 displayed extremely high overpotentials, Supplementary Figure S4, consistent with the poor continuity of the Pt films obtained from these depositions. Overall, the results are in general agreement with those of Papandrew *et al.*,[4] who also observed poor activity from Pt@CDP powders with 5 wt% Pt, Figure 6. Powders with 9 wt% Pt and higher displayed approximately fixed activity (i.e., independent of Pt wt%), and in further analogy to the present results, the electrocatalytic behavior was insensitive to Pt crystallite size. Those authors attributed poor oxygen electroreduction rates at low Pt loadings to discontinuity of the Pt

films resulting in poor electronic connectivity, a feature also evident in the low Pt content films prepared here.

From the comparison provided in Figure 6, it is evident that, although the trends between the two types of Pt@CDP powders are similar, the overpotentials of the ALD processed cathodes are somewhat greater than those of the MOCVD processed cathodes, by about 90 mV at a bias of 50 mA/cm^2. Even after accounting for an estimated 10 mV increase in the overpotential in the MOCVD processed cathodes that would be expected to accrue during 100 h of operation (for direct comparison to the ALD cathode measurement condition), the difference is noteworthy. The distinct properties may be due to the substantial difference in Pt crystallite size – in the range of 8 to 12 nm for the ALD approach, vs. 2.4 to 3.7 nm for the MOCVD approach. That is, while sensitivity may be limited within either of these two ranges, a four-fold difference in size may account for the differences between the two Pt deposition approaches. Alternatively, the difference in overpotentials may be due to the speculated loss in CDP surface area during ALD processing. Both possibilities are consistent with a proposed electrochemical reaction pathway in which protons or atomic hydrogen species migrate through the Pt film and undergo reaction with oxygen at the Pt-air interface, Figure 7. We have proposed an analogous pathway for hydrogen electro-oxidation on the surface of dense Pt thin films.[18]. In the case of oxygen electro-reduction, loss of CDP surface area would result in loss of active area, and loss of Pt grain boundaries would result in loss of possible hydrogen diffusion pathways or surface reaction sites. Despite the higher overpotential, the Pt utilization, defined here as $\left(\frac{1}{\eta(@\,50\mathrm{mA\cdot cm^{-2}})}\frac{1}{\mathrm{mg_{Pt}cm^{-2}}}\right)$ where $\eta(@\,50\mathrm{mA\cdot cm^{-2}})$ is the cathode overpotential at a current density of 50 mA·cm^{-2}, is somewhat higher for the ALD processed cathode Pt-200 (2.6

$cm^2 \cdot V^{-1} \cdot mg_{Pt}^{-1}$) than the best MOCVD processed cathode (2.0 $cm^2 \cdot V^{-1} \cdot mg_{Pt}^{-1}$, calculated from the data reported by Papandrew *et al.* [4]). This high utilization is achieved, in part, by limiting the overall mass of the cathode.

A key feature of the ALD processed cathodes is their excellent stability, as shown in the evolution of the cathode overpotential over time at a current density of 200 mA/cm^2, Figure 8. The Pt-300-#1 sample is particularly stable, undergoing a very slight decrease in cathode overpotential in the first 50 h of measurement, then remaining within 1 mV of 0.466 V for the subsequent 50 h. The Pt-250 and Pt-300-#2 samples similarly show initial slight improvements of about 10 mV followed by stable performance. In contrast, fluctuations in voltage are evident for the Pt-200 sample, which furthermore shows a slightly more pronounced average improvement in the first 50 h followed by a slightly more pronounced degradation in the latter 50 h. Over the entire 100 h measurement, the cathode overpotential of this sample increases by only 6 mV, but over the last 50 h the increase is 21 mV. These differences in voltage stability appear to be due to differences in the morphological evolution of the Pt coatings as shown in the post-measurement SEM images, Figure 9. In particular, some coarsening is evident in the case of the Pt-200 powder, whereas negligible morphological changes occur for Pt-250 and Pt-300. The present results are in general agreement with the (limited) stability studies performed by Papandrew et al. Those authors reported an average increase in overpotential of 110 μV/h for a cathode with a Pt loading of 9 wt % on CDP particles, along with a marked coarsening in the Pt after 200 h of measurement. In the present work, notable crystallite growth was observed over the course of the electrochemical measurements, Table 1 and Supplementary Figure S5, with crystallite size increasing by 50-65% across all samples. The virtually negligible impact on voltage of differences in Pt crystallite size, from 8 nm in the Pt-200 powder at the initiation of

the polarization measurements to 18 nm in the Pt-300 powder at the conclusion of the measurements, points towards CDP specific surface area rather than Pt crystallite size as the primary reason for the lower cathode overpotentials in the MOCVD deposited Pt. That is, for fixed CDP specific area, the present results demonstrate insensitivity of cathode overpotential to Pt crystallite sizes greater than 8 nm. Nevertheless, a possible benefit from substantially decreasing the Pt crystallite size cannot be ruled out.

4. Conclusions

Growth of Pt by atomic layer deposition on CsH_2PO_4 was achieved using trimethyl(methylcyclopentadienyl)platinum ($MeCpPtMe_3$) and ozone as the reagents. The growth occurs by a two-stage process. Slow nucleation and lateral growth, with almost negligible deposition, occurs in the first 80 cycles. Subsequently, after a more or less continuous film is formed, conventional layer-by-layer growth occurs at a growth rate of 0.09 ± 0.01 wt%/cycle, which corresponds to approximately 0.02 nm/cycle. Fully continuous films were obtained after 200 deposition cycles (8.6 wt% Pt). The Pt crystallite size increased from 8 to 12 nm upon increasing the number of deposition cycles from 200 to 300, and was found to be substantially larger than the estimated Pt film thickness, of 1.8 to 5.9 nm. The cathode overpotential in cells prepared using these Pt@CDP powders was relatively insensitive to the Pt loading on the CDP powders, measuring ~ 0.5 V for a current density of 200 mA/cm^2, so long as Pt film continuity was achieved. The overpotential as also largely insensitive to Pt crystallite size. Significantly, these cells demonstrated excellent stability as measured over a 100 h period, despite increases in Pt crystallite size by 50 to 65%. The general characteristics of these Pt@CDP powders are similar to those reported previously for analogous powders prepared by unconventional MOCVD

methods. The results support the proposal that hydrogen migrates through the Pt film and that the rate-limiting step in the overall electrochemical reaction occurs at one or both of the double-phase boundaries, the Pt-CDP and Pt-air interfaces, justifying fabrication strategies that aim to maximize the (Pt-coated) electrolyte specific surface area rather than the CDP-Pt-air triple-phase boundaries.

A key advantage of ALD over other deposition techniques, besides the highly conformal nature (which has been exploited here), is the precise control offered over film thickness. In the present system, the nucleation delay apparently contributes to challenges in taking advantage of the favourable linear growth characteristics. Thus, routes to ensuring reproducible nucleation behaviour will be the subject of future efforts. A second challenge encountered here is the low Pt yield, with less than 1% of the Pt supplied to the reaction resulting in deposition. Creative solutions to this obstacle will also be required if the promising characteristics of the ALD method are to be utilized in commercially relevant systems.

Acknowledgements

This research was supported by the U.S. Department of Energy, through ARPA-e contract DE-AR0000495 and the U.S. Department of Energy, Office of Science, Basic Energy Sciences, through grant number DE-FG02-87ER13808. The authors gratefully acknowledge the use of several user facilities at Northwestern University. Specifically, this work made use the EPIC facility of Northwestern University's NUANCE Center, which has received support from the Soft and Hybrid Nanotechnology Experimental (SHyNE) Resource (NSF ECCS-1542205); the MRSEC program (NSF DMR-1720139) at the Materials Research Center; the International

Institute for Nanotechnology (IIN); and the Keck Foundation; and the State of Illinois, through the IIN. This work also made use of the J. B. Cohen Diffraction X-ray Diffraction Facility supported by the MRSEC program of the National Science Foundation (DMR-1720139) at the Materials Research Center and the Soft and Hybrid Nanotechnology Experimental (SHyNE) Resource (NSF ECCS-1542205). Chemical analysis for metal content was performed at the Northwestern University Quantitative Bio-element Imaging Center.

References

[1] M. W. Louie, M. Kislitsyn, K. Bhattacharya, S. M. Haile, Phase transformation and hysteresis behavior in $Cs_{1-x}Rb_xH_2PO_4$, Solid State Ionics, 181(3-4) (2010) 173-179.

[2] S. M. Haile, C. R. I. Chisholm, K. Sasaki, D. A. Boysen, T. Uda, Solid acid proton conductors: from laboratory curiosities to fuel cell electrolytes, Faraday Discuss., 134 (2007) 17-39.

[3] C. R. I. Chisholm, D. A. Boysen, A. B. Papandrew, S. K. Zecevic, S. Y. Cha, K. A. Sasaki, A. Varga, K. P. Giapis, S. M. Haile, From laboratory breakthrough to technological realization: The development path for solid acid fuel cells, Electrochem. Soc. Interface, 18(3) (2009) 53-59.

[4] A. B. Papandrew, C. R. I. Chisholm, R. A. Elgammal, M. M. Ozer, S. K. Zecevic, Advanced Electrodes for Solid Acid Fuel Cells by Platinum Deposition on CsH_2PO_4, Chem. Mater., 23(7) (2011) 1659-1667.

[5] D. A. Boysen, T. Uda, C. R. I. Chisholm, S. M. Haile, High-performance solid acid fuel cells through humidity stabilization, Science, 303(5654) (2004) 68-70.

[6] T. Uda, S. M. Haile, Thin-membrane solid-acid fuel cell, Electrochem. Solid-State Lett., 8(5) (2005) A245-A246.

[7] V. Evoen, Electrocatalysis in Solid Acid Fuel Cells, Ph.D. Thesis, California Institute of Technology, California, United States, 2016.

[8] S. M. George, Atomic Layer Deposition: An Overview, Chem. Rev., 110(1) (2010) 111-131.

[9] J. Hamalainen, M. Ritala, M. Leskela, Atomic Layer Deposition of Noble Metals and Their Oxides, Chem. Mater., 26(1) (2014) 786-801.

[10] J. Hamalainen, F. Munnik, M. Ritala, M. Leskela, Atomic Layer Deposition of Platinum Oxide and Metallic Platinum Thin Films from $Pt(acac)_2$ and Ozone, Chem. Mater., 20(21) (2008) 6840-6846.

[11] J. Dendooven, R. K. Ramachandran, K. Devloo-Casier, G. Rampelberg, M. Filez, H. Poelman, G. B. Marin, E. Fonda, C. Detavernier, Low-Temperature Atomic Layer Deposition of Platinum Using (Methylcyclopentadienyl)trimethylplatinum and Ozone, J. Phys. Chem. C, 117(40) (2013) 20557-20561.

[12] A. Ikeda, S. M. Haile, The thermodynamics and kinetics of the dehydration of CsH_2PO_4 studied in the presence of SiO_2, Solid State Ionics, 213 (2012) 63-71.

[13] H. B. R. Lee, K. L. Pickrahn, S. F. Bent, Effect of O_3 on Growth of Pt by Atomic Layer Deposition, J. Phys. Chem. C, 118(23) (2014) 12325-12332.

[14] L. Baker, A. S. Cavanagh, D. Seghete, S. M. George, A. J. M. Mackus, W. M. M. Kessels, Z. Y. Liu, F. T. Wagner, Nucleation and growth of Pt atomic layer deposition on Al_2O_3 substrates using (methylcyclopentadienyl)-trimethyl platinum and O_2 plasma, J. Appl. Phys., 109(8) (2011) 084333.

[15] S. K. Kim, J. H. Han, G. H. Kim, C. S. Hwang, Investigation on the Growth Initiation of Ru Thin Films by Atomic Layer Deposition, Chem. Mater., 22(9) (2010) 2850-2856.

[16] J. W. Elam, A. V. Zinovev, M. J. Pellin, D. J. Comstock, M. C. Hersam, Nucleation and Growth of Noble Metals on Oxide Surfaces Using Atomic Layer Deposition, ECS Trans., 3(15) (2007) 271-278.

[17] B. D. Cullity, S. R. Stock, Elements of X-ray Diffraction. 3rd ed., Prentice Hall: New York, 2001.

[18] M. W. Louie, S. M. Haile, Platinum thin film anodes for solid acid fuel cells, Energy Environ. Sci., 4(10) (2011) 4230-4238.

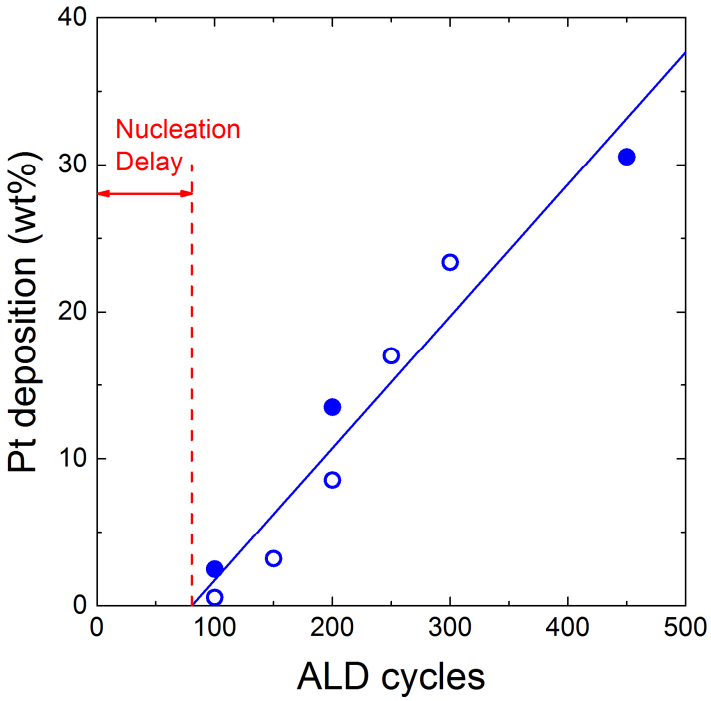

Figure 1. Pt deposition on CDP powder as a function of number of ALD cycles. The open symbols indicate Pt@CDP materials utilized in subsequent characterization, including fuel cell evaluation.

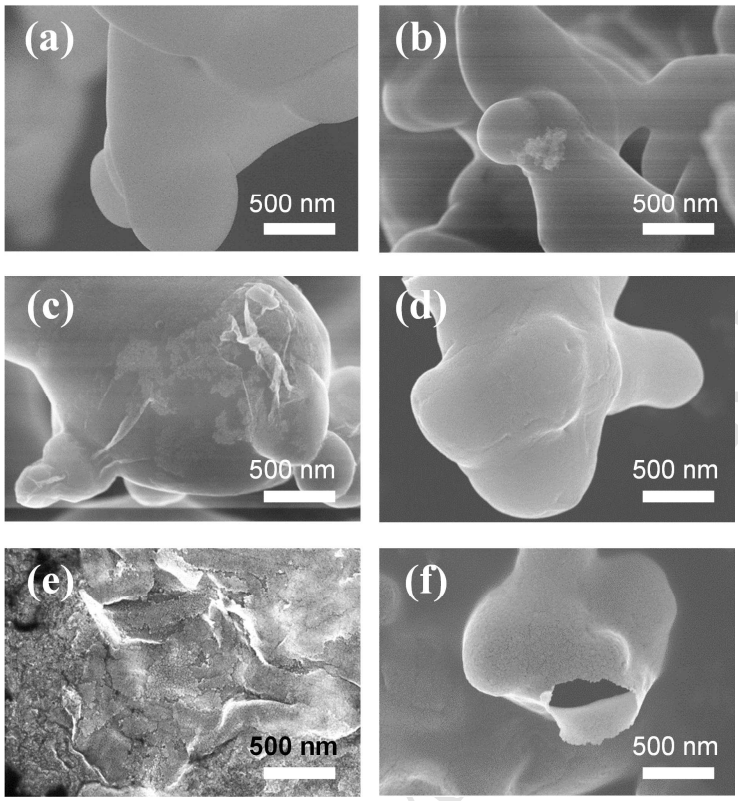

Figure 2. Scanning electron microscopy images showing nature of ALD-Pt on CDP: (a) bare CDP, (b) as-deposited Pt-100, (c) as-deposited Pt-150, (d) as-deposited Pt-200, (e) Pt-150 after dissolution of CDP, and (f) Pt-200 after dissolution of CDP.

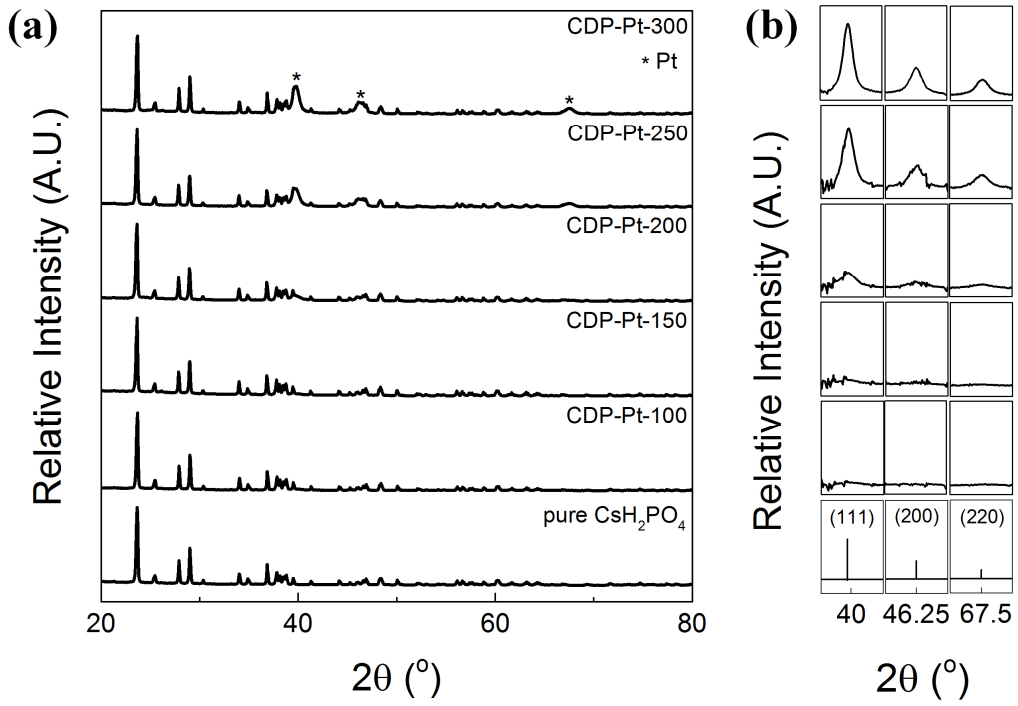

Figure 3. X-ray diffraction patterns from neat CDP and from as-prepared Pt@CDP particles: (a) raw diffraction patterns, and (b) residual peaks after subtraction of CDP pattern, revealing Pt peaks.

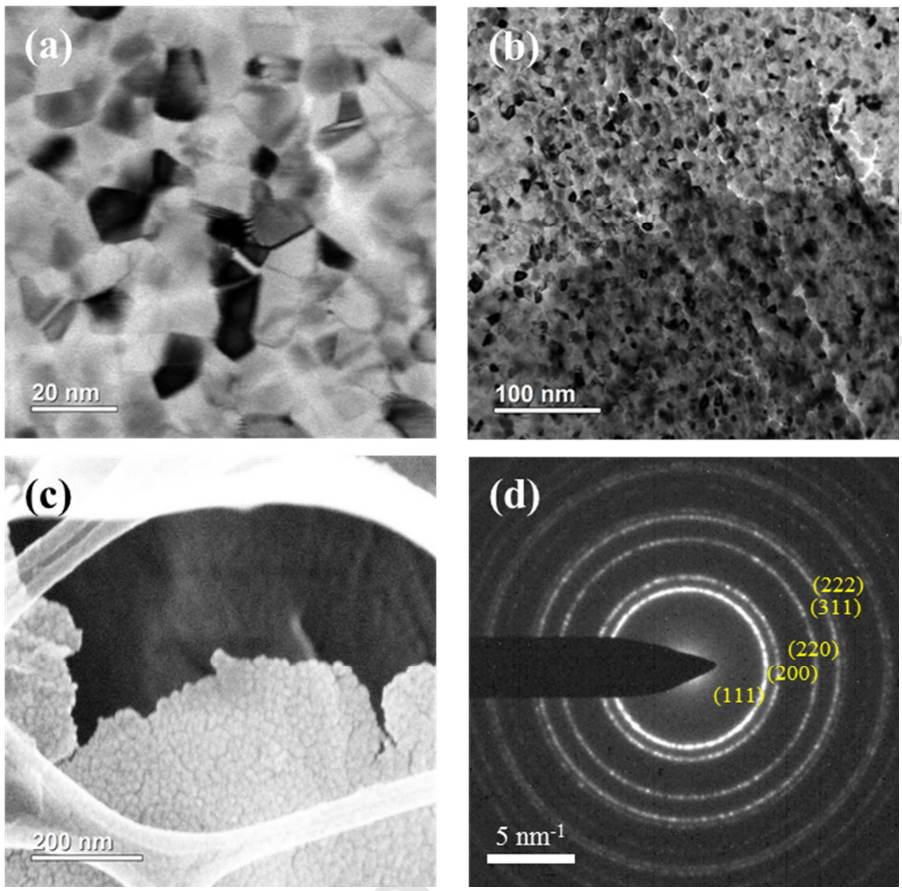

Figure 4. Electron microscopy images, at various magnifications, of Pt films from the Pt-200 material after dissolution of the underlying CDP: (a), (b) transmission electron microscopy images, (c) scanning electron microscopy image of the film on holey carbon substrate, and (d) selected area diffraction pattern (SADP). Variations in darkness of different grains in the TEM images are largely due to variations in grain orientation; they are not due to porosity in the film.

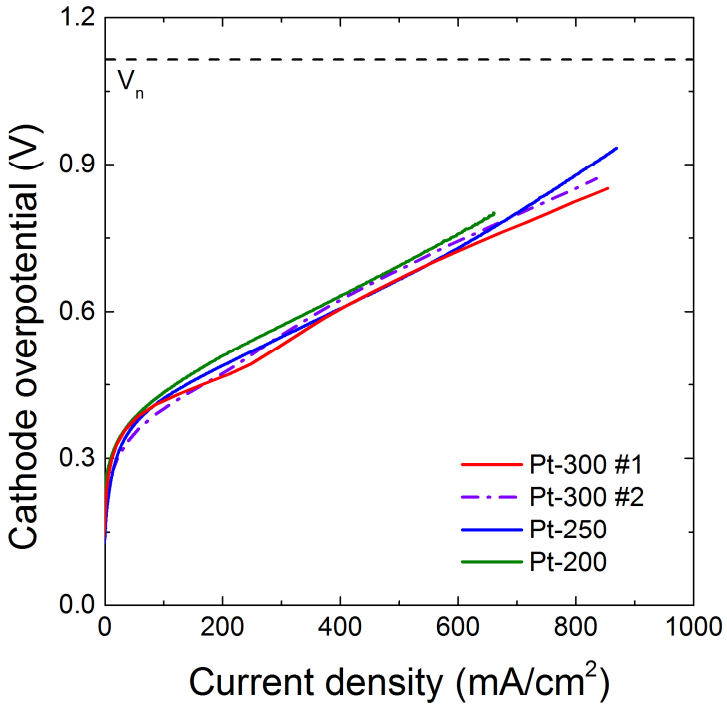

Figure 5. Cathode overpotentials in SAFCs with the cathode powders indicated, as measured after 100 h of operation at 250 °C with humidified hydrogen supplied to anode and humidified air supplied to cathode.

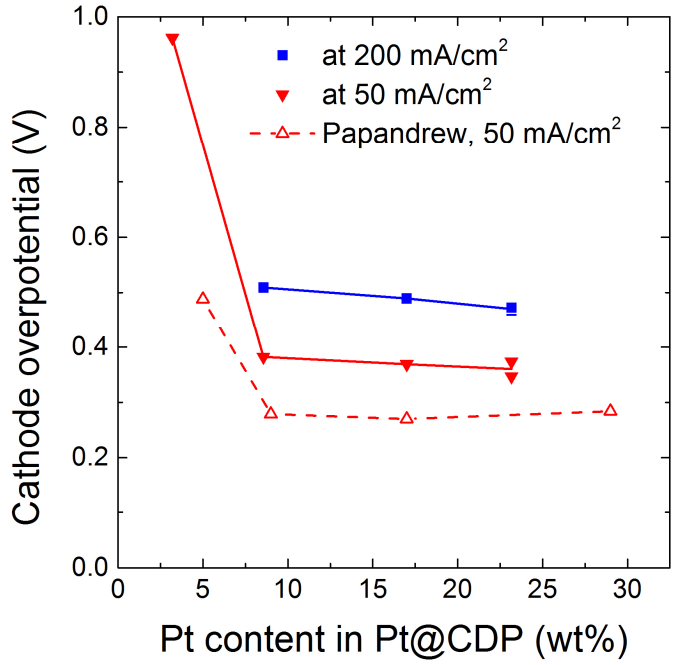

Figure 6. Cathode overpotentials at 50 and 200 mA/cm^2 as a function of Pt loading on CDP powders coated by ALD. Measurements are at 250 °C with humidified hydrogen supplied to anode and humidified air supplied to cathode, after 100 h of operation. The results reported by Papandrew et al. using cathodes prepared by MOCVD methods (without 100 h of operation)[4] are shown for comparison.

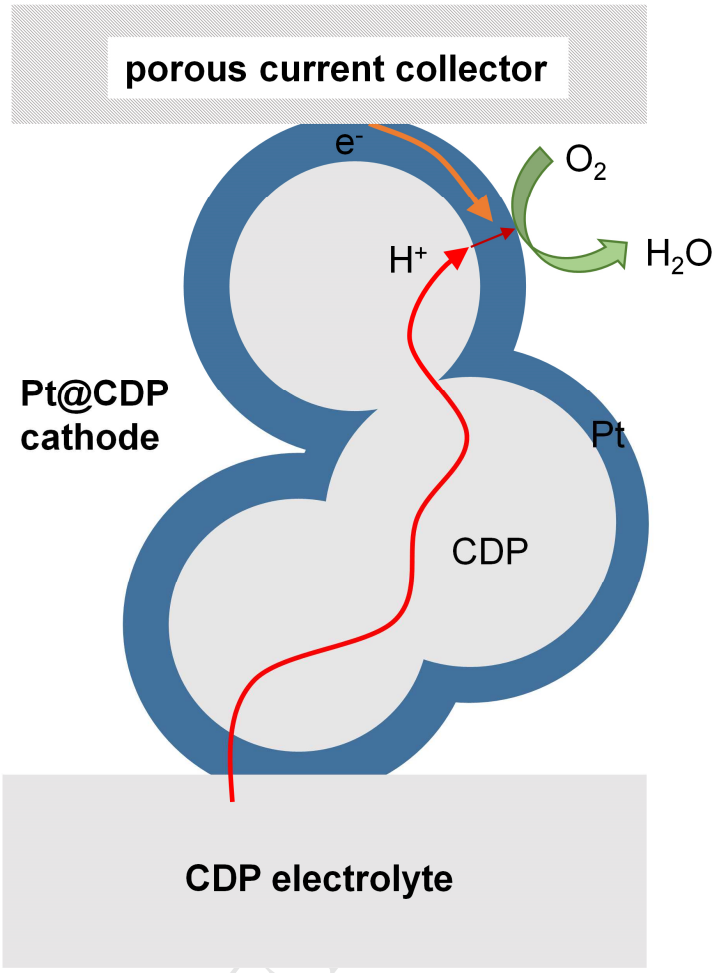

Figure 7. Schematic illustration of the proposed reaction pathway for oxygen electrooxidation on Pt@CDP, based on the analogous pathway demonstration for hydrogen electroreduction on dense Pt thin films.[18]

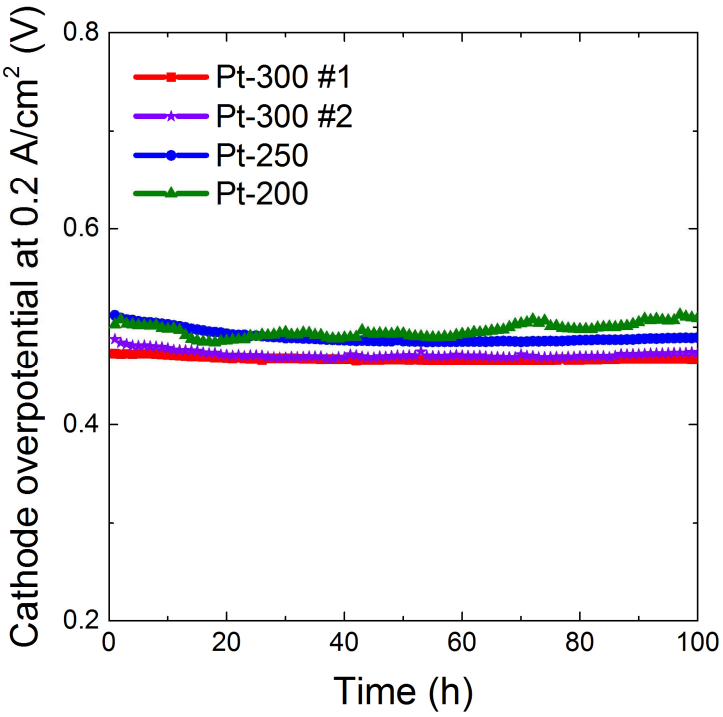

Figure 8. Temporal evolution of the cathode overpotentials at 200 mA/cm^2 for cells with cathode powder as indicated (measurement at 250 °C with humidified hydrogen supplied to anode and humidified air supplied to cathode).

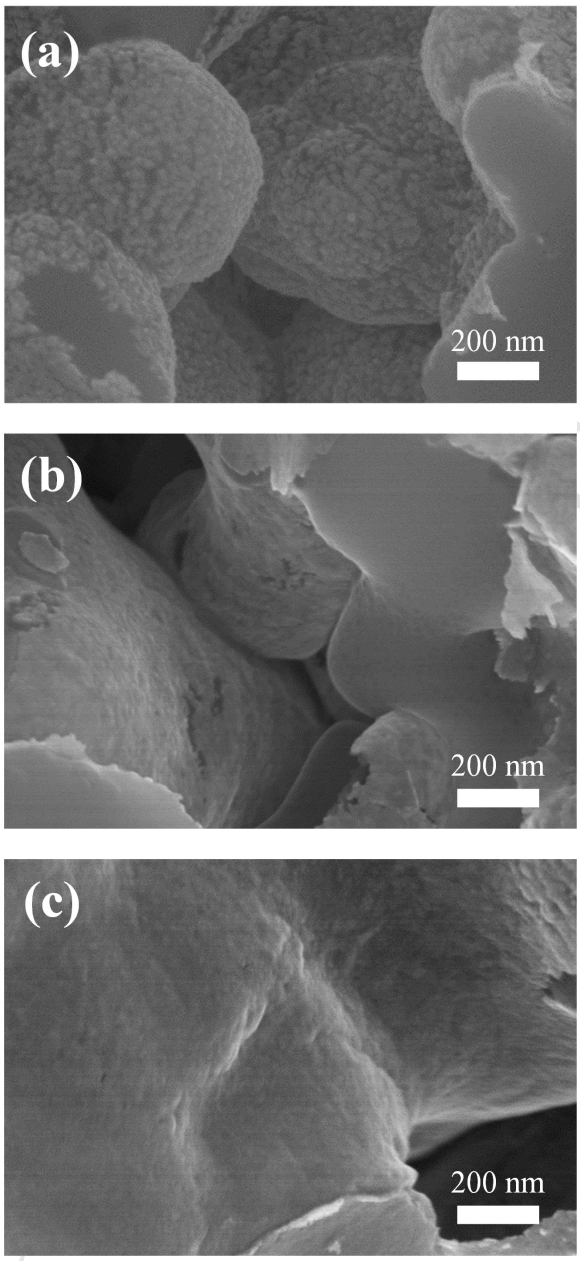

Figure 9. High resolution SEM images SAFC cathodes after 100 h operation: (a) Pt-200, (b) Pt-250, (c) Pt-300.

Table 1. Deposition amount, thickness and grain size of ALD Pt films as-coated onto CDP particles, and characteristics of cathodes prepared from the Pt@CDP powders.

Sample	Deposition (wt%)	Pt yield (%)	Thickness (nm)	Crystallite size (nm)**	Cathode mass (mg)	Pt loading (mg/cm^2)
Pt-100*	0.56	0.05	0.1	not detectable	50	0.1
Pt-150	3.20	0.18	0.6	not detectable	40	0.5
Pt-200*	8.56	0.38	1.8	8 (13)	33	1.0
Pt-250	17.00	0.66	4.0	10 (16)	36	2.2
Pt-300-1§	23.17	0.81	5.9	12 (18)	37	3.0
Pt-300-2§				12 (n/a)	50	4.1

* using Pt-100 and Pt-200 depositions that resulted in lower Pt yields.

§ prepared from the same Pt@CDP batch

** number in parentheses indicates crystallite size as measured after 100 h of electrochemical measurement.